Journal of Materials Chemistry A

Accepted Manuscript

This article can be cited before page numbers have been issued, to do this please use: B. Chong, W. Zhu and X. Hou, *J. Mater. Chem. A*, 2017, DOI: 10.1039/C6TA10202F.

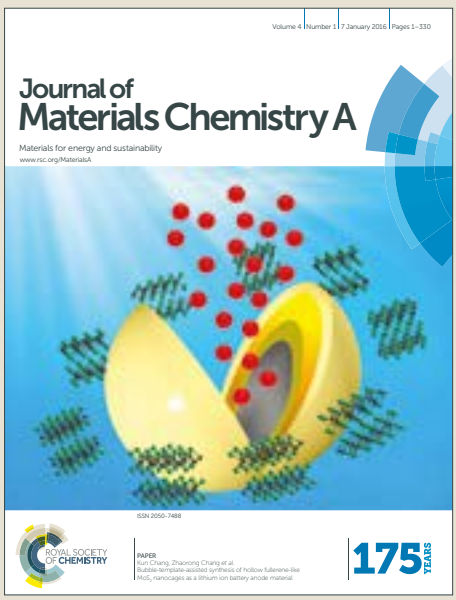

ROYAL SOCIETY OF CHEMISTRY

rsc.li/materials-a

View Article Online
DOI: 10.1039/C6TA10202F

Journal Name

RSCPublishing

ARTICLE

Epitaxial Hetero-structure of CdSe/TiO_2 Nanotube Arrays with PEDOT as hole transfer layer for photoelectrochemical hydrogen evolution

Cite this: DOI: 10.1039/x0xx00000x

Received 00th January 2012,
Accepted 00th January 2012

DOI: 10.1039/x0xx00000x

www.rsc.org/

Baohe Chong[ac], Wen Zhu*[abc], Xianghui Hou[b]

The photocatalytic decomposition of water is believed to be able to help mitigate the crisis of fossil fuel depletion. However, the photocatalytic hydrogen production remains challenge to obtain high and stable photoconversion efficiency. Here we report an epitaxial hetero-structure of CdSe/TiO_2 nanotube arrays as efficient photo-anodes via simple room-temperature, low-cost electrochemical deposition. With the help of the similar d spacing with TiO_2, CdSe sensitization layer is epitaxially grown on the tube wall of the TiO_2 nanotubes, resulting in an ideal coherent grain boundary and single crystal growth. The resultant photo-anode produces 30% more photocurrent than those samples without coherent grain boundary. Notably, the especial epitaxial hetero-structure is beneficial to decrease the recombination site and accelerate the separation of photogenerated electron-hole pairs. Furthermore, an ultrathin PEDOT surface layer was developed on the epitaxial hetero-structure of CdSe/TiO_2 nano-tube arrays in which it functions as both a physical passivation barrier and a hole transfer layer. As a result, significantly enhanced photocurrent density and substantially better stability have been achieved. This methodology may be providing a new pathway of epitaxial growth for preparing the heterogeneous junction materials which have similar d spacing.

Introduction

Photoelectrochemical water splitting is a significant way to produce hydrogen, which has been attracting intense attention because of the pressing need to solve energy crisis and environment problem. Since the seminal demonstration of photoelectrochemical cell (PEC) water splitting using TiO_2 by Honda and Fujishima in 1972,[1] extensive studies have been carried out on the TiO_2 nanomaterials due to its high photocatalytic activity, photochemical stability, nontoxicity and low cost.[2] In comparison with the traditional TiO_2 nanocrystal materials, one-dimensional nanostructured materials, such as nanotubes, nanorods[3] and nanowire,[4] are being more focused because of their enhancements in charge separation, charge transport, and light absorption. Among them, highly ordered, vertically oriented TiO_2 nanotube arrays (NTAs) prepared on a Ti foil by electrochemical anodization can offer larger specific surface areas without a concomitant decrease in geometric and structural order. The one-dimensional highly ordered nanotubular structure is more advantaged in the collection of charge carriers by building an attractive electron percolation path along the long axis of the nanotubes, allowing vectorial charge transfer between interfaces and thereby minimizing charge recombination.[5, 6] However, TiO_2 is a large band-gap semiconductor (3.2 eV), the photoresponse of TiO_2 is confined to the UV region which only accounts for less than 5% of the solar spectrum. To extend its photoresponse into visible light region, researchers have developed various strategies, such as doping of metal/nonmetal ions, surface sensitization of organic dyes/metal complexes, surface fluorination, and coupling with narrow band gap semiconductor (e.g. CdS,[7] CdSe,[8] CdTe,[9] PbS[10]). Especially, TiO_2 NTAs decorated with narrow bandgap semiconductors have been demonstrated to be a convenient system for light harvesting by virtue of efficient separation of charge carrier and more favourable energy band structure to match with the solar spectra.[11]

Among all kinds of narrow band-gap semiconductors, CdSe is considered to be one of the most promising counterparts with TiO_2 NTAs, on account of its excellent energy band-gap and good electron mobility. However, although CdSe has demonstrated its usefulness for solar-driven water splitting in numerous reports owing to its visible-light responsive band gap and high absorption coefficient, the sensitized TiO_2 NTAs with CdSe are generally considered to be unstable for long life

View Article Online
DOI: 10.1039/C6TA10202F Journal Name

application because of the inevitable photodegradation of transition-metal chalcogenides semiconductor in aqueous medium.[12] A variety of passivation coating such as ZnS,[13] Al_2O_3,[14] SiO_2,[15] or TiO_2[16] has been reported to prevent the degradation of metal chalcogenides semiconductor. However, all these inorganic coatings basically act as energy barriers to promote the recombination of photogenerated hole with electron in the nanostructured oxide. Such system generally isn't effective to accelerate the separation of photogenerated electron-hole pairs.[17]

To overcome this problem, the Poly (3, 4-ethylenedioxythiophene) (PEDOT), an effective organic hole conductor in light-emitting diodes and organic solar cells, is introduced into the CdSe/TiO_2 NTAs. PEDOT as a multi-functional coating has been reported to prevent photocorrosion of Si nanowires, collect photogenerated holes and catalyze the water oxidation reaction.[18] In the present study, the PEDOT coating is in-situ galvanostatic polymerization on the wall of CdSe/TiO_2 NTAs to synergistically prevent photo-degradation of CdSe and promote the hole-scavenging reactions by efficiently transferring photoinduced holes, and its stability for photocatalytic hydrogen production in long term illumination is investigated.

In addition, synthetic strategies toward CdSe/TiO_2 NTAs heterostructure are primarily confined to the following methods, namely, chemical bath deposition, hydrothermal synthesis, and spray pyrolysis deposition. Apart from these inevitably complicated and time consuming synthetic protocols, more importantly, in most cases, the deposition of CdSe ingredients on TiO_2 NTAs in conjunction with intimate interfacial interaction is far from satisfactory. The conventional methods for integrating CdSe coating layer to highly ordered TiO2 NTAs are usually inevitable to produce lattice distortion zone.[19-25] It is known that the grain boundary has been commonly considered as the main carrier recombination site in nanocrystalline photoelectrodes. Besides, these boundaries also lower the electron transport rate and heighten the energy losses. In contrast, a modified Electrochemical atomic layer deposition (ECALD) method can overcome these obstacles. The ECALD method as reported in the literature is based on underpotential deposition (UPD).[26-30] UPD is a surface-limited phenomenon in which the deposition of one element occurs at a potential that precedes the Nerstian equilibrium value, so that the resulting deposit is generally limited to one atomic layer. ECALD utilizes alternating UPD of the elements that form the compound semiconductor in a cycle. Each deposition cycle can form only a monolayer of heterogenous elements, and the thickness of the deposit is controlled by the number of deposition cycles. To date, ECALD has been wildly used to grow structurally well-ordered compound semiconductors with atomic-level control at ambient temperature and pressure.[31-34] Obviously, the growth mechanism of ECALD gives rise to good interactions between the deposition layer and the NTAs (the interface properties from the atom-by-atom contact form) and as a result enables efficient and rapid charge transfer through the coupled semiconductor.

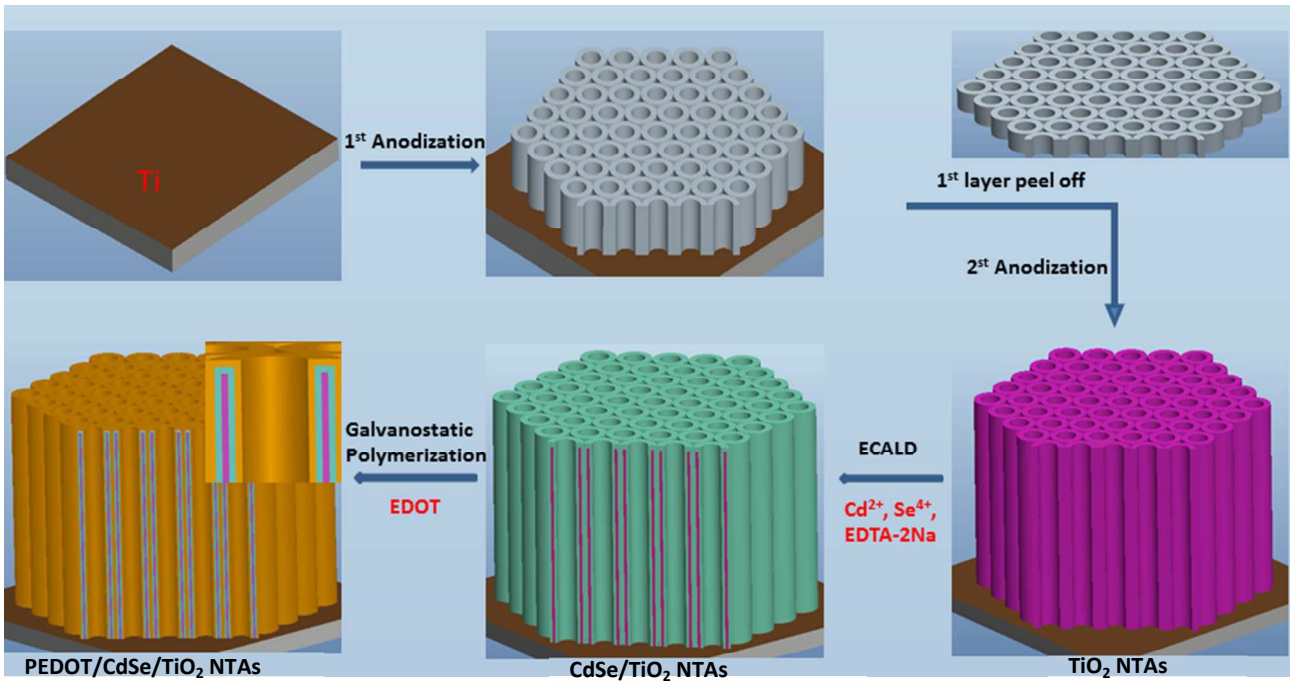

Figure 1. Flowchart illustrating the fabrication process of the PEDOT/CdSe/TiO_2 NTAs hetero-structure.

Journal Name View Article Online DOI: 10.1039/C6TA10202F ARTICLE

Experimental

Preparation of TiO_2 NTAs. Synthesis of highly ordered TiO_2 NTAs followed the typical two-step anodic oxidation method. Titanium foils (99.8% purity) were mechanically ground using emery papers with different types and polished with metallographic abrasive paper successively, then ultrasonically cleaned orderly with acetone, distilled water and ethanol, followed by drying in ambient air (at laboratory temperature and common ambient pressure). The anodization of titanium foil was carried out in an electrolyte comprised of NH_4F (0.32 wt.%) and distilled H_2O (2.0 vol%) in ethylene glycol at room temperature using platinum foil as the counter electrode. The two-step anodic oxidation was conducted as follows: step-1, the titanium foil was firstly anodized at 54V for 20 minutes in the electrolyte, followed by rinsing with ethanol and drying in ambient air, then by annealing at 700℃ in muffle furnace for 1h with heating rate of 7℃/min; step-2, the sample was re-soaked into the electrolyte and suffered the second anodization for 11 hours, then was annealed again at different temperature (200℃; 300℃; 450℃; 700℃) to investigate the effect of temperature on epitaxial growth.

Fabrication of Coaxial Hetero-structure of CdSe/TiO_2 NTAs. For electrochemical ALD of CdSe on TiO2 NTAs, $CdSO_4$ (10mM) and SeO_2 (2mM) with analytical reagent grade were used as the sources of Cd and Se, respectively. EDTA-2Na($C_{10}H_{14}O_8N_2Na_2 \bullet 2H_2O$) and NH_4OH were used to complex the ions and adjust the pH value for obtaining a proper electrodeposition potential. The solutions were freshly prepared just before the beginning of each series of measurements. The electrochemical ALD was carried out using a computer controlled electrochemical workstation that was connected to a three-electrode system comprised of TiO_2 NTAs as work electrode (WE), Pt foil as counter electrode (CE) and Hg_2Cl_2/KCl (SCE) as reference electrode (RE). After deposition, the CdSe coupled TiO_2 NTAs were then annealed again at 450℃ to obtain the coaxial heterogeneous nanojunction sample of CdSe/TiO_2 NTAs.

Electropolymerization of PEDOT.

The polymerization solution contained 0.1 M $LiClO_4$ and 0.01 M monomer (EDOT, bis-EDOT) in acetonitrile, and the three-electrode system was used for electropolymerization of PEDOT, where CdSe/TiO_2 NTAs as working electrode, and SCE and platinum foil were used as reference and counter electrodes, respectively. Galvanostatic polymerization method was used for electropolymerization of PEDOT, and the current was 0.5mA. All solutions were de-aerated by purging N_2 through the solution for 30 min prior to polymerization.

Characterizations. The morphologies of the samples were observed through field emission scanning electron microscopy (FESEM) (Nova NanoSEM 450) and transmission electron microscopy (TEM) (JEOL JEM-2100). The X-ray diffraction (XRD) (X'Pert PRO) measurement was performed using a Bruker D8 diffractometer with Cu Ka radiation operated at 40 kV, 40 mA. The UV-vis absorption spectra were collected at room temperature using Lambda 35 UV-vis spectrophotometer. For the incident-photon-to-current-conversion efficiency (IPCE) measurement, light source was generated by a 300W xenon lamp of Newport(Oriel,69911) and then split into specific wavelength using Newport oriel cornerstone 130 1/8 Monochromator (Oriel, model 74004).

The optical response performance of the samples was investigated in a photoelectrochemical cell with platinum foil counter electrode and SCE reference electrode. The CorrtestTM CS350 electrochemical workstation was also used to control the potential and record the photocurrent generated. An aqueous solution containing 0.24 M Na_2S and 0.34 M Na_2SO_3 was used as a testing electrolyte and sacrificial hole scavenger in photoelectrochemical measurements. The measurements were done under Xe lamp (CHF-XM35-500W) illumination. Xe lamp coupled to an AM 1.5G filter was used as the standard light source throughout the tests. The illumination area was 1.0 cm×2.0 cm. The illumination intensity of 100mW/cm^2 was calibrated with a readout meter for solar simulator irradiance before the measurement.

Results and discussion

Epitaxial Heterostructure of CdSe/TiO_2 Nanotube Arrays

A two-step anodization method was applied to grow highly ordered TiO_2 NTAs (see the Experimental Section for more details). Different annealing temperature was chosen to study its influence on the growth of CdSe sensitizing layer. Samples with four various annealing temperature were prepared, that are marked as TiO_2 NTAs (200°C), TiO_2 NTAs (300°C), TiO_2 NTAs (450°C) and TiO_2 NTAs (700°C). Figure S1 shows the top-view FE-SEM images of as-prepared samples of TiO_2 NTAs (300°C) and TiO_2 NTAs (700°C). The TiO_2 NTAs (300°C) sample presented a highly uniform array of nanotubes of 100 nm in diameter and about 10 nm in wall thickness. In comparison with the TiO_2 NTAs (300°C) sample, the TiO_2 NTAs (700°C) sample has a broken tube wall, suggesting that the thin tube wall can't stand high annealing temperature. Therefore, annealing temperature above 700°C is not suitable for further sensitization with CdSe. Figure S2 shows XRD patterns of the pure TiO_2 NTAs with different annealing temperature. All diffraction peaks in TiO_2 NTAs (200°C) can be well-indexed to Ti metal phase, indicating that the crystal structure of TiO_2 NTAs is amorphous due to the low annealing temperature. After raising the annealing temperature to 300°C and 450°C, the diffraction peaks of TiO_2 phase appear. The diffraction peaks in TiO_2 NTAs(450°C) is more intense than that in TiO_2 NTAs(300°C), indicating that the TiO_2 NTAs(450°C) has a better crystallinity. In addition, two sharp diffraction peaks at 25.16° and 37.76°, which are assigned to (101) and (004) reflection of tetragonal anatase (I41/amd, PDF 21−1272), indicate a preferred orientation growth along the two lattice planes.

CdSe sensitized layer was successfully deposited on pure TiO_2 NTAs substrate to form a coaxial heterogeneous structure of nanotube-array by ECALD. The details of UPD process of CdSe sensitized layer were described in our previous work.[35, 36] By using proper UPD parameter, CdSe sensitizer is homogeneously covered on both interior and exterior wall surfaces of TiO_2 NTAs without any obvious particle agglomeration, suggesting the ECALD method in our work is rather efficient to grow well dispersed nanofilms among the whole nanotube wall. Figure S3 shows the top-view FE-SEM images of as-prepared sample CdSe/TiO_2 NTAs. After TiO_2 NTAs are coated with CdSe sensitized layer, the inner diameter of the NTs decreases from 100 nm to 80 nm, and thus the thickness of CdSe coating layer is calculated to be about 10 nm. EDX elemental mapping analysis gives the distribution of

View Article Online
DOI: 10.1039/C6TA10262F
Journal Name

elements of Ti, O, Cd and Se, confirming the even distribution of CdSe coating (Figure S4). Figure 2 shows XRD patterns of the CdSe/TiO_2 NTAs(300°C) and the CdSe/TiO_2 NTAs(450°C) samples. After decorating TiO_2 NTAs with CdSe, some new diffraction peaks located at 24.13°, 42.34°, and 49.93° appear. These new peaks are correspondingly attributed to (100), (110), and (112) of hexagonal CdSe (P63mc, PDF 65-3415), conforming that the CdSe coating layer possesses a hexagonal crystal structure.

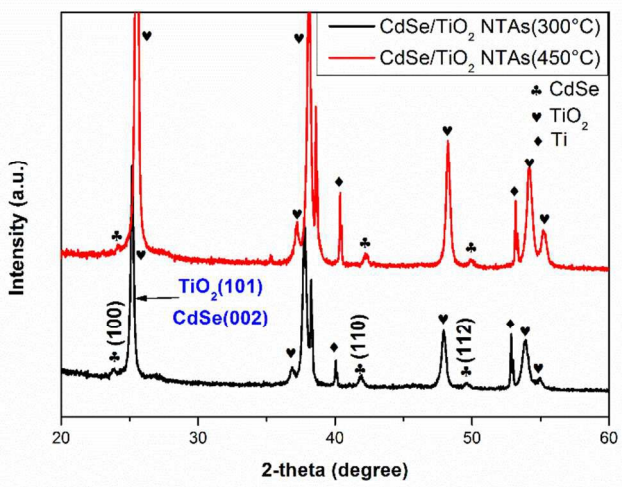

Figure 2. XRD diffractograms of samples: (black line) CdSe/TiO_2 NTAs(300°C); (red line) CdSe/TiO_2 NTAs(450°C)

The morphology of both TiO_2 and CdSe/TiO_2 was probed by TEM. Figure 3a and 3b feature the single pure TiO_2 nanotube that is annealed at 300°C and 450°C, respectively. The pure nanotube shows a hollow nanostructure and has a wall thickness of about 10 nm which is significantly less than the carrier diffusion length (ca. 20 nm in TiO_2), thus ensures the efficient separation of charge carrier.[7, 37] Their HRTEM images are shown in Figure 3d and 3e. The d spacing of 0.237 nm was identified to the interplanar spacing of (004) plane for pure TiO_2 nanotube sample annealed at 300°C, while the d spacing of 0.352nm was the interplane spacing of (101) plane for sample annealed at 450°C. This phenomenon is consistent with the XRD results in which the (101) and (004) planes are those planes with highly oriented growth. Figure 3c and 3g show the TEM images of CdSe/TiO_2 (300°C) and CdSe/TiO_2 (450°C), respectively. The semiconductor of CdSe was found to grow uniformly on the inner and outer wall of TiO_2 nanotube. In comparison with pure TiO_2 nanotube, the wall thickness of the coated nanotube with CdSe increased by 10 nm, indicating that the thickness of CdSe film is about 10 nm. Figure 3f features the HRTEM image of CdSe/TiO_2 (300°C) in which a very good layer stack structure was found. The inner layer has a d spacing of 0.352 nm to designate the interplanar spacing of the TiO_2 (101) plane. It is interesting to notice that the outer nanocrystal layer has an approximately equal d spacing with the inner layer (0.351 nm), which matches well with the interplanar spacing of CdSe (002) plane and is consistent with the XRD measurement results shown in Figure 2. Most importantly, CdSe is epitaxial growth along the plane (101) of TiO_2, no crystal boundary between the TiO_2 and CdSe phase is observed. The selected-area electron diffraction (SAED) pattern of CdSe/TiO_2 (300°C) nanotube is shown in the insert map of Figure 3f. A superimposed pattern of single crystalline composite material is obvious. Structurally, CdSe has three fastest growth directions of <0001>, <01$\bar{1}$0>, and <2$\bar{1}\bar{1}$0>, which is common in hexagonal wurtzite structures.[38, 39] The incident electron beam is along <0001> that implies the CdSe growth along <0001>. However, for the hexagonal wurtzite structure, the interplanner distance of 0.351 should indicate the growth along <2$\bar{1}\bar{1}$0>. The spot 2 and spot 3 marked in the SAED pattern is consistent with the growth direction of <0001>, but the spot 1 was measured to be 0.35nm, which matched well with the interplanar spacing of the CdSe(002) plane and was consistent with the growth direction of <2$\bar{1}\bar{1}$0>. We believed that these two coexisting growth directions in SAED pattern should be attributed to the epitaxial growth of CdSe on TiO_2. Analogical phenomenon has also been discovered in TiO_2 growth from $H_2Ti_3O_7$.[40] As shown in Figure 2, the peaks of CdSe(002) and TiO_2(101) have the same location in XRD pattern, the same interplanner distance implies that CdSe could epitaxially grow on TiO_2.

On the contrary, as shown in Figure 3h and 3i, obvious lattice distortion about 3nm thickness between the TiO_2 and CdSe phase was found from the sample of CdSe/TiO_2 (450°C). Such lattice distortion area will be the recombination central of photogenerated electrons and holes. Figure 3h and 3i feature two typical regions on the tube wall of CdSe/TiO_2 (450°C) sample. In figure 3h, The d spacing of 0.237 in the inner layer was identified to the interplanar spacing of the TiO_2(004) plane. The d spacing in the outer nanocrystal layer was measured to be 0.215 nm, which matched well the interplanar spacing of the CdSe(110) plane. In figure 3i, The d spacing of 0.352 in the inner layer is the interplanar spacing of the TiO_2(101) plane, while the d spacing of 0.371 nm in the outer nanocrystal layer is used to designate the interplanar spacing of the CdSe (100) plane. All these orientations are consistent with the XRD measurement results shown in Figure 2.

Since both CdSe/TiO_2 (300°C) and CdSe/TiO_2 (450°C) samples have a same secondary annealing at 450 °C after deposition of CdSe, why does CdSe/TiO_2 (300°C) sample show an epitaxial hetero-structure but CdSe/TiO_2 (450°C) sample have an obvious lattice distortion? The reason must be due to the different original characteristic of TiO_2 substrate in the composite nano-structural crystal samples. It is known that a large amount of junction defects can exist in the interface area between sensitizer and substrate during the formation of composite nano-structural crystal. It has been found that annealing is one approach to reduce the dislocation density in the interface of composite material.[41] In comparison with CdSe/TiO_2 (300°C) sample, TiO_2 substrate in CdSe/TiO_2 (450°C) have a higher annealing temperature at 450°C, which results in even more stable interface defect that can't be optimized through secondary annealing. However, the TiO_2 substrate with low annealing temperature at 300°C in CdSe/TiO_2 (300°C) sample has a susceptible interface characteristic which can be healed by the secondary annealing at 450°C, as a result enables an epitaxial hetero-structural interface between the sensitizer CdSe and TiO_2 substrate. This epitaxial hetero-structure, to some extent, needs to be considered for accelerating electron-hole separation/transport and reducing losses of carrier

Journal Name

View Article Online
DOI: 10.1039/C6TA10202F

recombination.[42, 43] The analogical phenomenon also was discovered in CdSe/TiO_2 (200°C) sample, in which the TiO_2 substrate was annealed at more low temperature of 200°C. Figure S5 show the TEM images of TiO_2 (200°C) and CdSe/TiO_2 (200°C) fabricated through depositing CdSe on TiO_2 NTAs (200°C) by ECALD method. TiO_2 (200°C) (Figure S5b) shows an amorphous due to the low annealing temperature, which is consistent with XRD result shown in Figure S2. After depositing CdSe on TiO_2 NTAs(200°C) and secondary annealing at 450°C, The sample shows a coaxial hetero-structure (Figure S5c). The enlarged HRTEM image taken at the junctions of the CdSe and TiO_2 substrate (Figure S5d) revealed that CdSe is also epitaxially grown on the TiO_2 tube wall while the corresponding FFT pattern confirms its single-crystallinity of the formed CdSe nanofilm.

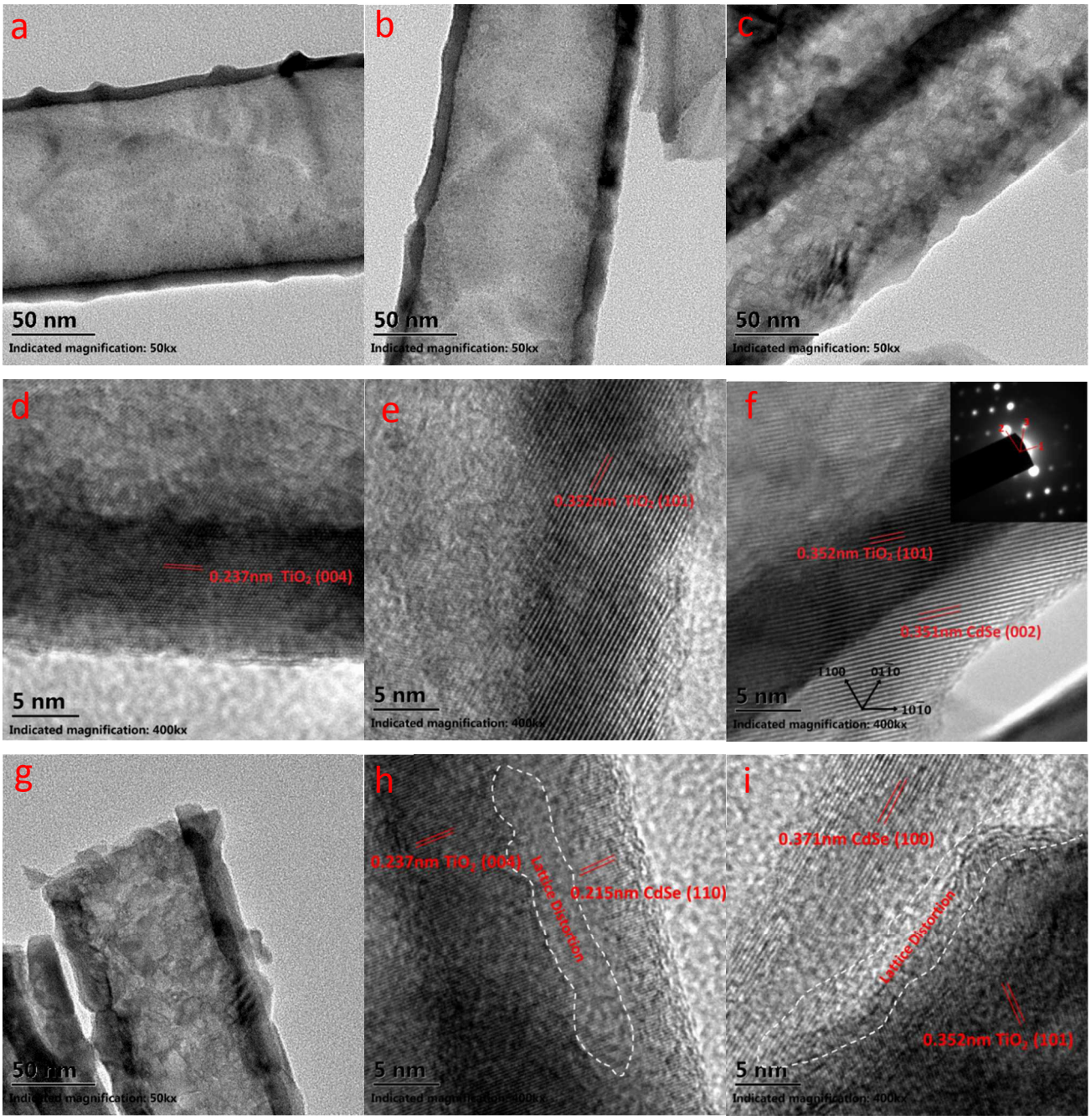

Figure 3. TEM and HRTEM images of samples. (a, d) TiO_2 NTAs(300°C); (b, e) TiO_2 NTAs(450°C); (c, f) CdSe/TiO_2 NTAs(300°C); (g-i) CdSe/TiO_2 NTAs(450°C)

Figure 4 shows the photocurrent density versus potential curves and corresponding photocurrent response under pulsed illumination with a bias voltage kept at -0.5V Vs. SCE for all samples. The stable photocurrent density of pure TiO_2 (300°C) and TiO_2 (450°C) was about 1.5 mA/cm^2 and 1.75 mA/cm^2, respectively (the current density is measured against the

View Article Online
DOI: 10.1039/C6TA10202F
Journal Name

projected area of the TiO_2 NTAs). After deposition of CdSe on the TiO_2 NTAs using the electrochemical ALD method, the improvement of photocurrent densities of CdSe/TiO_2 NTAs was obvious. In particular, CdSe/TiO_2 NTAs(300°C) shows a better enhancement in the photocurrent density than CdSe/TiO_2 NTAs(450°C). Furthermore, as shown in Figure 4a, the increasing slope of photocurrent density in CdSe/TiO_2 NTAs(300°C) sample is larger than that in CdSe/TiO_2 NTAs(450°C) sample. This might be attributed to the epitaxial growth of CdSe on TiO_2 NTAs(300°C) that built an unhindered transfer path for photogenerated electrons and holes. As shown in Figure 4b, for CdSe/TiO_2 NTAs(300°C) sample, the photocurrent first reached 8.5 mA/cm^2 and then dropped to a stable value of 7.5 mA/cm^2. This slight dropping of photocurrent implies that carriers have accumulated on the photoanode surface once being illuminated. Such accumulation of carriers owes to the rapid photo-generation efficiency in CdSe/TiO_2 NTAs(300°C) sample, which increased the capacitance of the photoanode/electrolyte interface. As the accumulated carriers were transmitted, the photocurrent became steady.

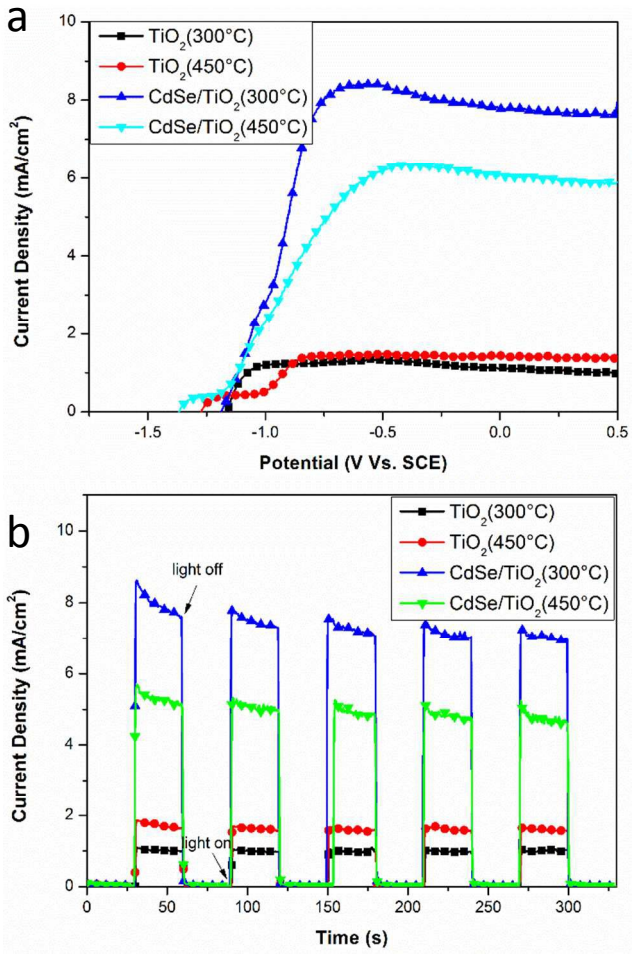

Figure 4. Photocurrent density versus potential curve measured for different samples. (b) Photocurrent response under pulsed illumination with a bias voltage kept at -0.5 V Vs. SCE.

Electropolymerization of PEDOT coating on CdSe/TiO_2 NTAs

The CdSe/TiO_2 NTAs(300°C) electrode was then selected as the optimal seed layer for PEDOT electropolymerization on account of its best photocurrent density. The conventional method for integrating the PEDOT coating to highly ordered nano-materials is constant voltage electropolymerization.[44, 45] In general, constant voltage electropolymerization easily leads to the precipitation of the coatings inside the nanotubes or even plugging the nanotubes, resulting in decreases in the specific surface area and adsorption capacity. The difficulty in microstructural control might be attributed to the change of surface information of nanotubes in the wake of the electropolymerization of PEDOT. Figure 5a shows the Cyclic voltammogram of the CdSe/TiO_2 NTAs(300°C) electrode recorded at 10 mV/s in solutions containing 0.01 M EDOT.

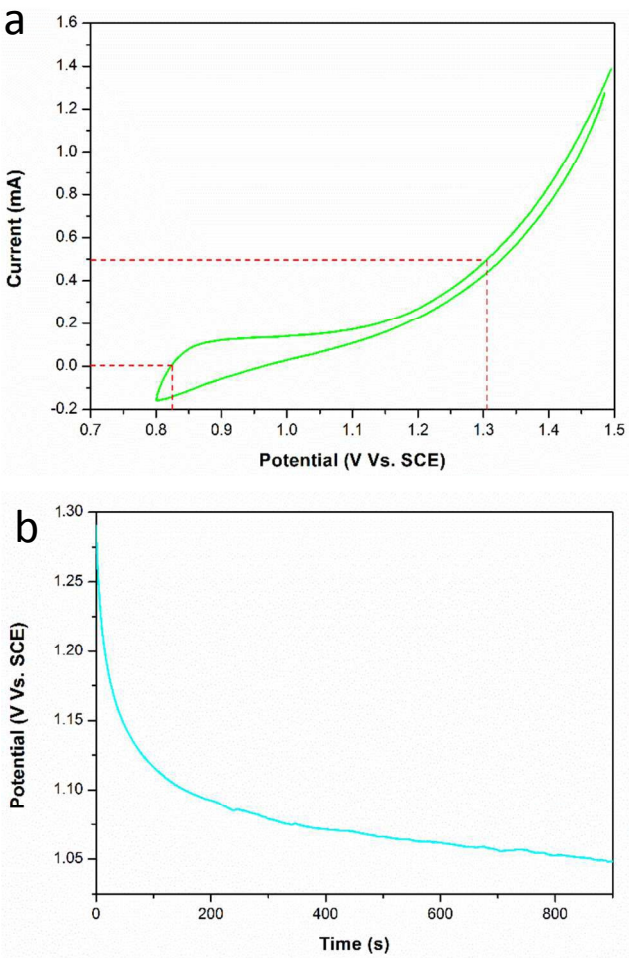

Figure 5. (a) Cyclic voltammogram of the CdSe/TiO_2 NTAs(300°C) electrode recorded at 10 mV/s in solutions containing (green line) 0.01 M EDOT; (b) Potential versus time measured in galvanostatic polymerization process.

It reveals that an oxidation current starting at about 0.8V vs. SCE. However, the polymer only began to noticeably coat at around 1.2 V as evidenced by the fast current increase. The positive current obtained by positive potential scan on the CV is also indicative of the nucleation/ growth mechanism expected for electrochemical polymerisation.[44] For controlling the rate of electropolymerization accurately, galvanostatic(500uA) polymerization method was used for

Journal Name

View Article Online
DOI: 10.1039/C6TA10202F ARTICLE

electropolymerization of PEDOT in this work. Figure 5b shows the potential versus time measured in the galvanostatic polymerization process. As shown in Figure 5b, the potential decreases rapidly between 0s to 200s, indicating that the PEDOT gradually covered the naked surface of $CdSe/TiO_2$ NTAs(300°C). The surface of $CdSe/TiO_2$ NTAs(300°C) was fully covered at 200s, then the electrode resistance slowly decreased owing to the growth of PEDOT in thickness.

Figure S6 shows the FESEM images of $PEDOT/CdSe/TiO_2$ NTAs. It revealed that the PEDOT uniformly covered onto the NT surface without aggregation. PEDOT polymer coating was confirmed by using flourier transform infrared spectroscopy (FTIR) analyses (Figure 6). The band at 1521.98cm^{-1} is associated with C=C asymmetric stretching vibration. The peak at 1323.13cm^{-1} corresponds to C-C stretches of the thiophene ring. The peaks at about 1187.84 and 1088.98cm^{-1} are assigned to the C-O-C band stretching vibration, while the peak at 976.87cm^{-1} is the C-S stretching vibration. All of these peaks can be attributed to the role of PEDOT coating on $CdSe/TiO_2$ NTAs, except the peak of 836.20 cm^{-1} which is associated with the band of TiO_2, indicating that PEDOT was successfully electrodeposited on $CdSe/TiO_2$ NTAs. This FTIR spectrum of synthesized PEDOT is consistent with reported literatures.[46-48]

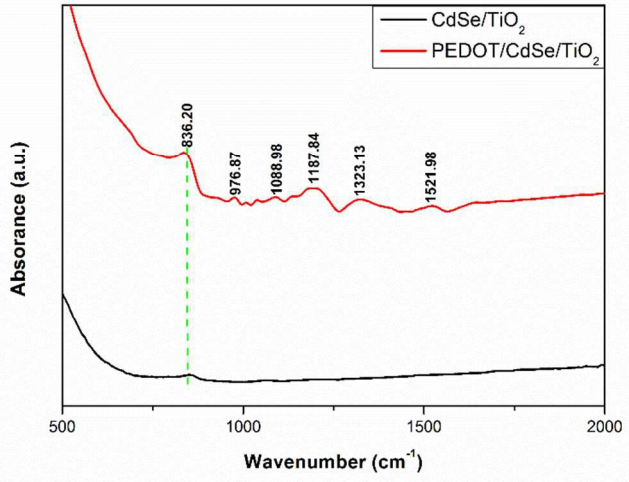

Figure 6. FTIR spectra of $CdSe/TiO_2$ and $PEDOT/CdSe/TiO_2$.

Figure 7a shows the XRD pattern of $PEDOT/CdSe/TiO_2$ NTAs. All diffraction peaks can be well-indexed to the CdSe phase, anatase TiO_2 phase and the Ti metal phase. Compared with the XRD pattern of $CdSe/TiO_2$ NTAs shown in Figure 2, the only difference was a broad diffraction centered approximately at 25°, which is associated to the coating layer of PEDOT on $CdSe/TiO_2$ NTAs, suggesting an amorphous state of PEDOT. The EDX elemental spot analysis was performed on coated $CdSe/TiO_2$ NTAs with PEDOT and the results are shown in Figure 7b. The elements of Ti and O confirm the presence of TiO_2, while Cd and Se peaks that were clearly visible on the EDX spectrum come from the CdSe deposit. Quantitative analysis of the EDX spectrum revealed that the atomic ratio of Cd (2.29%) versus Se (2.36%) was nearly 1, indicating that the deposited CdSe had the expected 1 : 1 stoichiometry. In addition, the elemental peaks of C and S were corresponds to PEDOT coating over the $CdSe/TiO_2$ NTAs. Also, the PEDOT coating is further probed by EDX mapping and the results are shown in Figure S7. The mapping clearly revealed that the $CdSe/TiO_2$ NTAs surface was uniformly coated with PEDOT.

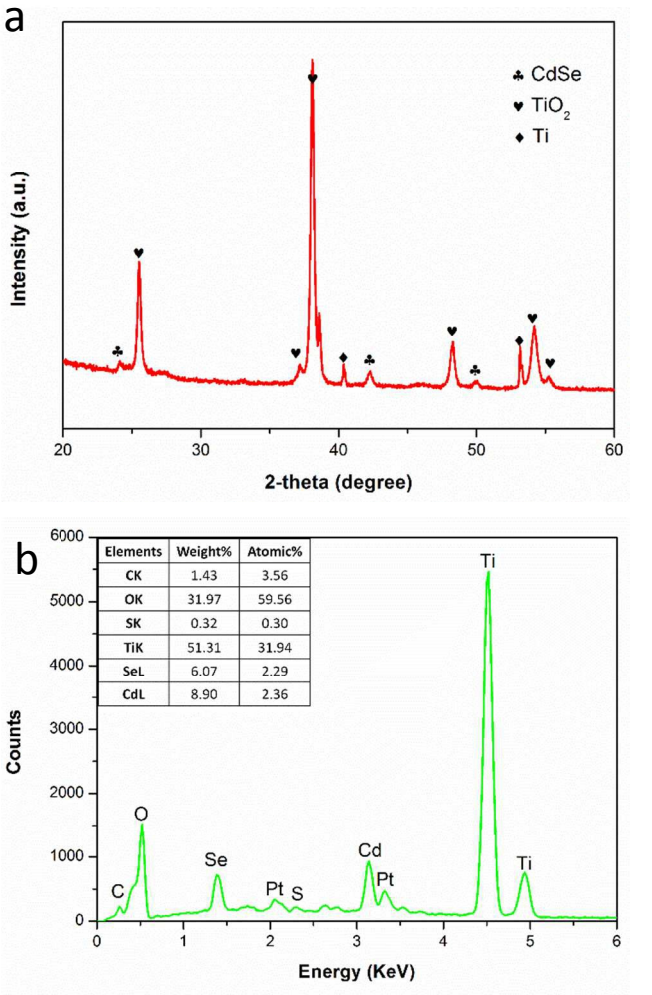

Figure 7. (a) XRD diffractograms of sample $PEDOT/CdSe/TiO_2$ NTAs; (b) EDX spectrum and the corresponding element content of sample $PEDOT/CdSe/TiO_2$ NTAs.

The photocurrent–potential curves measured on a series of $PEDOT/CdSe/TiO_2$ NTAs samples with various polymerization time for PEDOT are shown in Figure 8; data for the corresponding $CdSe/TiO_2$ NTAs substrate before polymerization is also provided. After electro-polymerization of PEDOT on the $CdSe/TiO_2$ NTAs, a noteworthy enhancement in the photocurrent density was found on the $PEDOT(10min)/CdSe/TiO_2$ NTAs sample in which the EDOT polymerized for 10min. As shown in Figure 8, the photocurrent density increases in the wake of the increasing PEDOT polymerization time within 10min. However, when the polymerization time was further increased to 15min, the photocurrent density dropped, indicating that the PEDOT layer was too thick after 15min of polymerization. Excessive PEDOT reduced light absorption because of the increase of photons transmission distance. The photoresponse experiments also show that the photo-excited current of all as-prepared samples coated with PEDOT is almost dominant and the charge transport in these material proceeds rapidly (Figure 8b). Notably, the dark current of sample $PEDOT(15min)/CdSe/TiO_2$

View Article Online
DOI: 10.1039/C6TA10262F
Journal Name

NTAs was almost 1.75mA/cm^2, which was associated to excessive PEDOT polymerization, indicating that a suitable thickness of PEDOT coating layer is significant for the transfer of photogenerated holes.

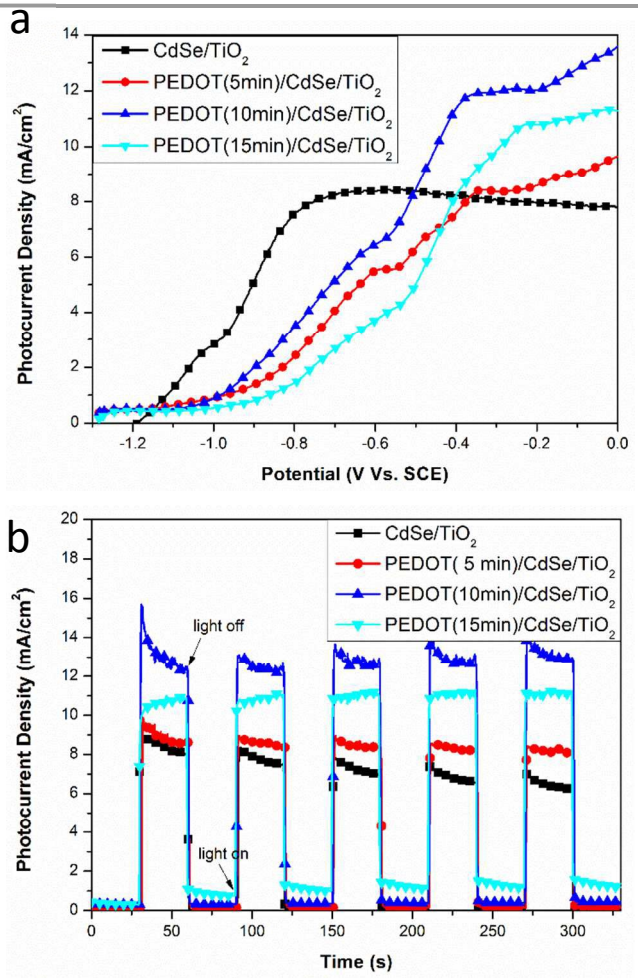

Figure 8. Photocurrent density versus potential curve measured for different samples. (b) Photocurrent response under pulsed illumination with a bias voltage kept at 0 V Vs. SCE.

Figure 9 illustrates the photogenerated electron–hole separation process and the photocatalytic redox reactions of the PEDOT/CdSe/TiO_2 heterogeneous for photoelectreochemical hydrogen evolution. The ideal step band edge structure for efficient transports of photogenerated charge-carriers in PEDOT/CdSe/TiO_2 electrode is shown in Figure 9b. When CdSe and TiO_2 were irradiated by visible light with a photon energy greater than their band gap energy, electrons are photoexcited from the valence band to the conduction band, leaving holes in the valence band. Subsequently, the photoexcited electrons are rapidly injected from the conduction band of CdSe to the conduction band of the TiO_2 NTAs , owing to the intimate interface and the less negative conduction band of TiO_2 NTAs as compared to that of CdSe. Meanwhile, the photoinduced holes are injected from the valence band of TiO_2 NTAs to the valance band of CdSe. In the end, all photoexcited holes migrate to the sensitizer-electrolyte interface and participate in the oxidation reaction. A cross section of a single coated coaxial heterogeneous structure showing the charge-transfer mechanism is displayed in Figure 9c. The highly ordered one-dimensional nanostructure provides a unidirectional electrical channel for charge transfer, so that photoinduced electron–hole pairs can be effectively separated and the photoexicited electrons are transferred to back-contact rapidly.[49, 50]

In an ideal case, a photoanode material should have an enough large band-gap energy in order to split water, in which its conduction band-edge energy and valence band-edge energy straddle the electrochemical potentials $E^0(H^+/H_2)$ and $E^0(O_2/H_2O)$, respectively, so that the generated electrons/holes can drive the hydrogen and oxygen evolution reactions under illumination (see in Figure 9b).[51] For our photoanode in this work, although the valence band-edge energy of CdSe is not more positive than the electrochemical potential $E^0(O_2/H_2O)$, however, the Fermi-level alignment between TiO_2 and CdSe has been proposed to construct a stepwise structure of band-edge levels, and as a result, the valence band-edge of CdSe will be moved toward more positive beyond the electrochemical potential $E^0(O_2/H_2O)$. Furthermore, the photoexcited holes will accumulate in the outer layer of PEDOT coating due to its valence band-edge energy is more negative than that of CdSe. In this regard, PEDOT plays a role of highly active hole scavengers, in which photogenerated holes irreversibly oxidize the reducing reagent instead of the oxygen evolution of water, and give rise to the enhanced photocatalytic performance of the PEDOT/CdSe/TiO_2 heterostructure. As being mentioned in the experiment section, the photo-electrochemical tests were conducted in the presence of Na_2S/Na_2SO_3 aqueous solution that can act as a sacrificial electrolyte and provide a great advantage to avoid the recombination of the photogenerated electron-hole pairs.

The open-circuit voltage-decay (OCVD) method is a way to probe the kinetics of recombination during the relaxation from illuminated quasi-equilibrium state to the dark equilibrium. Basically, OCVD is a dark measurement of the photo-electrode and hence only recombination is measured.[9] The termination of continuous irradiation results in a decay of Voc, which reflects the decrease of the interfacial charge concentration in the photoanode.[25] This process is an indication of the susceptibility of the interfacial charge accumulated in the photoanode to recombination.[52] As shown in figure S8, the photopotential of the PEDOT/CdSe/TiO_2 NTA photoelectrode is much higher than that of the un-coating CdSe/TiO_2 NTAs, indicating a greater accumulation of photogenerated charges. The lifetime of charge carriers is obtained by the reciprocal of the derivative of the decay curve normalized by potential.[53, 54] The photo potential decays slowly after returning the sample to the dark, indicating the long e^--h^+ lifetime which is consistent with the hole transfer character of PEDOT, namely, the PEDOT/CdSe/TiO_2 NTAs electrode exhibits longer lifetime of charge carriers compared with the CdSe/TiO_2 NTAs electrode. Hence PEDOT/CdSe/TiO_2 NTAs electrodes have slower kinetics of recombination and as a result enable higher photocurrent.

Electrochemical analysis also was carried out to investigate the charge transfer properties of samples. Figure S9 displays the Mott-Schottky-type plot of capacitance measurement in both

Journal Name View Article Online DOI: 10.1039/C6TA10202F ARTICLE

samples of $CdSe/TiO_2$ and $PEDOT/CdSe/TiO_2$. All samples are n type semiconductors because of the positive slopes of the C^{-2}-E lots.[53] Further, the order of the donor density, measured from the slope of the plots, follows a trend: $PEDOT/CdSe/TiO_2$ > $CdSe/TiO_2$, which is consistent with the result of the photocurrent density measurement. Another important parameter derived from the measurement is the flat band potential. It can be obtained from Figure S9 that the flat band potentials (V_{fb}) of $CdSe/TiO_2$ and $PEDOT/CdSe/TiO_2$ are -0.88V and -1.09V vs. SCE, corresponding to -0.64V and -0.85V vs. normal hydrogen electrode (NHE), respectively. For n-type semiconductors, the conduction band potentials (V_{CB}) are more negative by ~-0.1 V to their flat band potentials. Thereby, the V_{CB} of CdSe and PEDOT are about -0.74V and -0.95V vs. NHE, respectively. The valence band potentials (V_{VB}) of CdSe and PEDOT are about 0.86V and 0.55V vs. NHE, respectively, according to the formula $Eg = V_{VB} - V_{CB}$. In order to be seen clearly, the V_{fb}, V_{CB} and V_{VB} of all samples are summarized and shown in Table S1.[54-56] According to the experimental results of flat band potential test, the energy band positions of CdSe and PEDOT and electron transfer process in CdSe–PEDOT system can be illustrated in Figure S10.

As we know, an important step for photoelectrochemical evolution reaction is the generation and separation of electron–hole pairs. The transfer of charge carriers in the photocatalytic process is very important, which would inhibit the recombination of electrons and holes and increase the photocatalytic activity. The stepwise structure of band-edge levels provides a smooth pathway for electron-hole transfer. The PEDOT as a hole transfer material can effective improve the separation of photoexcited electron-hole pair, resulting in the accumulation of the photoexcited holes in the outer layer of PEDOT. In this regard, PEDOT plays a role of highly active hole scavengers and give rise to the enhanced photocatalytic performance of the $PEDOT/CdSe/TiO_2$ photoanode.

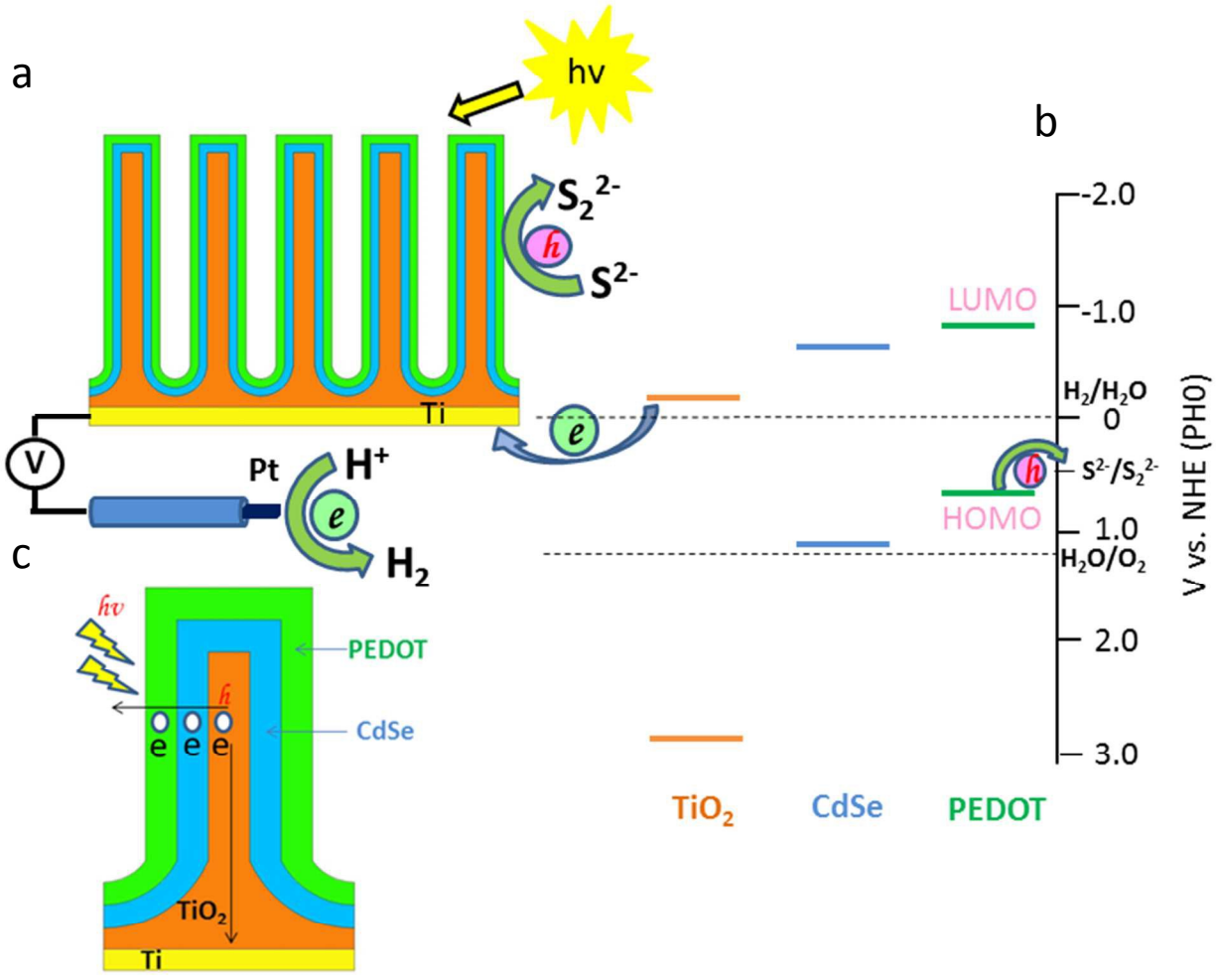

Figure 9. (a)Schematic illustration of proposed mechanism of the $PEDOT/CdSe/TiO_2$ coaxial heterogeneous for photo-electrocatalytic hydrogen evolution; (b) Ideal step band edge structure for efficient transports of photogenerated charge-carriers in $PEDOT/CdSe/TiO_2$ electrode; (c)Cross section of $PEDOT/CdSe/TiO_2$ coaxial heterogeneous and the charge-transfer mechanism.

View Article Online
DOI: 10.1039/C6TA10262F Journal Name

Figure 10a shows the UV-vis absorption curves of the pure TiO_2 NTAs, the CdSe/TiO_2 NTAs and the PEDOT/CdSe/TiO_2 NTAs. It can be seen that CdSe deposition atop TiO_2 NTAs has a red-shifted absorption edge in the visible region, and extends the absorption tail to 775 nm with a band-gap of about 1.6 eV corresponding to the typical band-gap value of CdSe. After PEDOT coating, the absorption has no further red-shifted but the absorbance of the cascade structural PEDOT/CdSe/TiO_2 NTAs is apparently stronger than that of the CdSe/TiO_2 NTAs in the visible region from 700 to 1000 nm. The enhanced absorbance is believed to be caused by the PEDOT coating layer, which belongs to the kind of polymer having a longer conjugation length with greater order and polaron and/or bipolaron bands.[48]

To quantify the photoresponse of the prepared samples, incident-photon-to-current-conversion efficiency (IPCE) measurements were made in which their photoresponses as a function of incident light wavelength are examined. As revealed in Figure S11, pure TiO_2 showed a response only in the UV light region with a maximum IPCE value of 21% obtained around 320nm. The CdSe/TiO_2 sample showed a pronounced response in the visible light region, with IPCE value of 32% obtained between 400nm and 600nm. The photoresponses of PEDOT/CdSe/TiO_2 were drastically extended to the all visible light regions of the solar spectrum after coating PEDOT on CdSe/TiO_2, indicating that PEDOT can promote the photoresponse owing to its narrow bad-gap and the capability of trapping holes.

Figure 10b shows the Nyquist curve of CdSe/TiO_2 (300°C) and PEDOT(10min)/CdSe/TiO_2 (300°C) samples measured in dark condition and under visible-light illumination. All Nyquist plots display a hemisphere at high frequencies whose diameter represents the electron-transfer resistance controlling the kinetics at the electrode surface. The straight line occurred at low frequency is related to the diffusion process. Evidently, the charge-transfer resistance in dark condition is larger than in visible-light illumination for all samples. Under light illumination, the charge transfer resistance of sample CdSe/TiO_2 (300°C) and PEDOT(10min)/CdSe/TiO_2 (300°C) is 152 $\Omega*cm^2$ and 89 $\Omega*cm^2$, respectively. The smaller charge transfer resistance in sample PEDOT(10min)/CdSe/TiO_2 (300°C) is consistent with its higher photocurrent density compared with CdSe/TiO_2 (300°C). The EIS measurement gives strong evidence that the conformal coating of PEDOT can greatly improve the charge transfer properties and display efficient separation of photoexcited electron–hole pair.

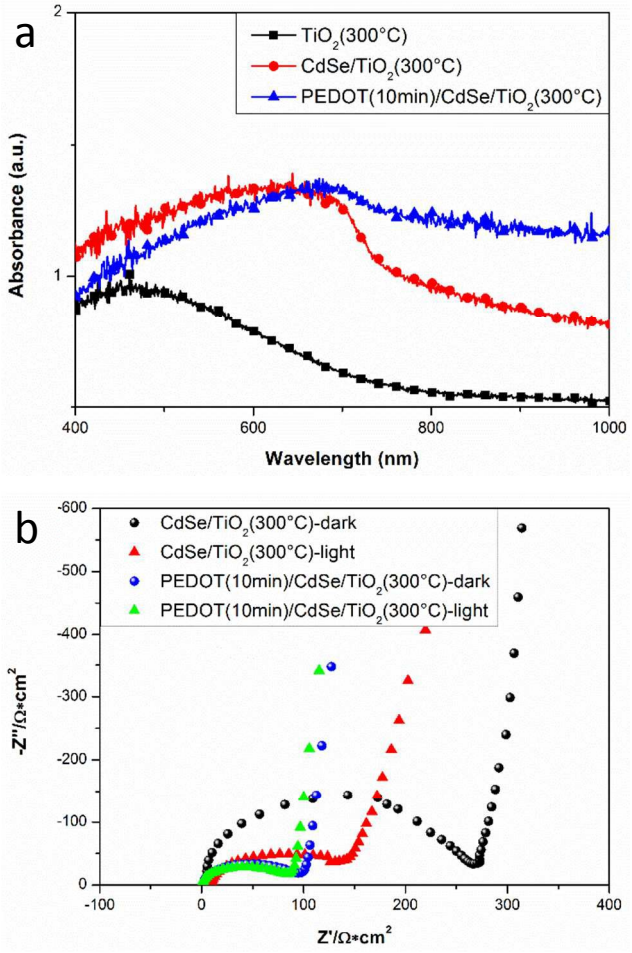

Figure 10. (a) UV-vis absorbance spectra of TiO_2 (300°C)(black line); CdSe/TiO_2 (300°C)(red line); PEDOT(10min)/CdSe/TiO_2 (300°C)(blue line); (b) EIS Nyquist plots for CdSe/TiO_2 (300°C) and PEDOT(10min)/CdSe/TiO_2 (300°C) under dark condition and visible-light illumination.

The stability of hydrogen generation was investigated through measuring photocurrent over time under light illumination. Table S2 shows some excellent investigation of catalytic stability in other photoelectrochemical system. It is observed that the transition-metal chalcogenides semiconductor is still the lack of long life stability for practical application under continuous illumination. Figure 11 shows the stability curves of CdSe/TiO_2 NTAs and PEDOT/CdSe/TiO_2 measured at basis potential of 0V Vs. SCE. For CdSe/TiO_2 NTAs electrode, the initial photocurrent density was 9mA/cm^2. That value markedly deteriorated to 4mA/cm^2, only being 44% of its initial value, after 3.5h of continuous illumination. However, for PEDOT-coated CdSe/TiO_2 NTAs electrode, the photocurrent density was more stable than uncoated CdSe/TiO_2 NTAs electrode. The improvement of stability thanks to the role of PEDOT coating that accepts photogenerated holes from CdSe, and as a result effectively inhibits the oxidative degradation of CdSe. It has been reported that PEDOT is an effective organic hole conductor in light-emitting diodes and organic solar cells, and is extremely stable in the presence of water or oxygen molecules.[47]

Journal Name

View Article Online
DOI: 10.1039/C6TA10202F ARTICLE

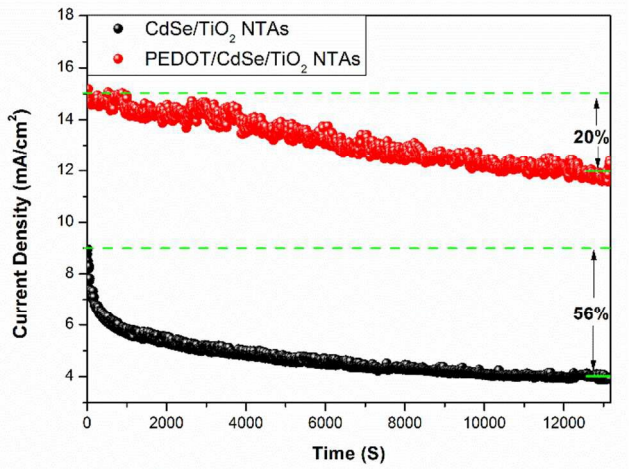

Figure 11. Photo stability of $CdSe/TiO_2$ NTAs and $PEDOT/CdSe/TiO_2$ measured at basis potential of 0V Vs. SCE.

Conclusions

We have designed a simple and unique method to prepare epitaxial hetero-structure of $CdSe/TiO_2$ nanotube arrays. This method combines all three processes, including the low temperature annealing, ECALD and the integrative annealing, to produce an epitaxial coaxial heterogeneous cascade structure. Such epitaxial hetero-structural photoanode produced 30% more photocurrent than common un-epitaxial samples. The enhanced photocurrent was attributed to the epitaxial interface between two heterogenous phases that can decrease the recombination site and accelerate the separation of photogenerated electron-hole pairs. We believe that this method could open up a new possibility in preparing hetero-structured materials with epitaxial growth. Additionally, we have developed the coated $CdSe/TiO_2$ photoanode with an ultrathin PEDOT surface layer, which functions as both physical passivation barrier and hole transfer layer. The PEDOT coating increased the photocurrent stability by accepting photogenerated holes from CdSe, thereby effectively inhibiting the oxidative degradation of CdSe. After 3.5h of continuous illumination, the photocurrent density of $PEDOT/CdSe/TiO_2$ NTAs retains 80% of initial value.

Acknowledgements

This work was financed by the Marie Curie IIF Fellowship (623733), the National Natural Science Foundation of China (21173090), the Special Found for Strategic Emerging Industry Development of Shenzhen (JCYJ20120618100557119). Technical assistance from the Analytical and Testing Center of HUST is gratefully acknowledged.

Notes and references

[a] State Key Laboratory of Materials Processing and Die & Mould Technology, Huazhong University of Science & Technology, Wuhan 430074, People's Republic of China

[b] Faculty of Engineering, The University of Nottingham, Nottingham NG7 2RD, UK

[c] Research Institute of Huazhong University of Science & Technology in Shenzhen, Shenzhen Virtual University Park, Shenzhen 518000, People's Republic of China

* Correspondence to: W. Zhu, State Key Laboratory of Materials Processing and Die and Mould Technology, Huazhong University of Science and Technology, Wuhan 430074, People's Republic of China. Tel./fax: +86 27 87558476.

* Corresponding author. Tel./fax: +86 27 87558476.

E-mail address: wennar@mail.hust.edu.cn (W. Zhu)

Electronic Supplementary Information (ESI) available: Additional figures showing the FESEM images of TiO_2 NTAs(300°C) and TiO_2 NTAs(700°C), XRD patterns of TiO_2 NTAs(200°C), TiO_2 NTAs(300°C)and TiO_2 NTAs(450°C), FESEM and EDX elemental mapping images of sample $CdSe/TiO_2$ NTAs(300°C), TEM and HRTEM images of samples of $CdSe/TiO_2$ NTAs(200°C), FESEM and EDX mapping images of $PEDOT/CdSe/TiO_2$ NTAs(300°C), OCVD , M-S and IPCE images of $CdSe/TiO_2$ and $PEDOT/CdSe/TiO_2$. See DOI: 10.1039/b000000x/

1. A. Fujishima, *Nature*, 1972, **238**, 37-38.
2. X. Chen and S. S. Mao, *Chem. Rev.*, 2007, **107**, 2891-2959.
3. A. Wolcott, W. A. Smith, T. R. Kuykendall, Y. Zhao and J. Z. Zhang, *Small*, 2009, **5**, 104-111.
4. G. Wang, H. Wang, Y. Ling, Y. Tang, X. Yang, R. C. Fitzmorris, C. Wang, J. Z. Zhang and Y. Li, *Nano lett.*, 2011, **11**, 3026-3033.
5. D. Wang and L. Liu, *Chem. Mater.*, 2010, **22**, 6656-6664.
6. J. H. Park, S. Kim and A. J. Bard, *Nano lett.*, 2006, **6**, 24-28.
7. F.-X. Xiao, J. Miao, H.-Y. Wang and B. Liu, *J. Mater. Chem. A*, 2013, **1**, 12229-12238.
8. F.-X. Xiao, J. Miao, H.-Y. Wang, H. Yang, J. Chen and B. Liu, *Nanoscale*, 2014, **6**, 6727-6737.
9. H. Yang, W. Fan, A. Vaneski, A. S. Susha, W. Y. Teoh and A. L. Rogach, *Adv. Funct. Mater.*, 2012, **22**, 2821-2829.
10. Q. Kang, S. Liu, L. Yang, Q. Cai and C. A. Grimes, *ACS Appl. Mater. Interfaces*, 2011, **3**, 746-749.
11. X. Li, J. Yu, J. Low, Y. Fang, J. Xiao and X. Chen, *J. Mater. Chem. A*, 2015, **3**, 2485-2534.
12. S. J. Moniz, S. A. Shevlin, D. J. Martin, Z.-X. Guo and J. Tang, *Energy Environ. Sci.*, 2015, **8**, 731-759.
13. H. Yang and P. H. Holloway, *Adv. Funct. Mater.*, 2004, **14**, 152-156.
14. K. E. Roelofs, T. P. Brennan, J. C. Dominguez, C. D. Bailie, G. Y. Margulis, E. T. Hoke, M. D. McGehee and S. F. Bent, *J. Phys. Chem. C*, 2013, **117**, 5584-5592.
15. Z. Liu, M. Miyauchi, Y. Uemura, Y. Cui, K. Hara, Z. Zhao, K. Sunahara and A. Furube, *Appl. Phys. Lett*, 2010, **96**, 233107.
16. M. Shalom, S. Dor, S. Ruhle, L. Grinis and A. Zaban, *J. Phys. Chem. C*, 2009, **113**, 3895-3898.
17. R. Liu, Z. Zheng, J. Spurgeon and X. Yang, *Energy Environ. Sci.*, 2014, **7**, 2504-2517.
18. X. Li, W. Lu, W. Dong, Q. Chen, D. Wu, W. Zhou and L. Chen, *Nanoscale*, 2013, **5**, 5257-5261.

View Article Online
DOI: 10.1039/C6TA10202F Journal Name

19. Q. Wang, S. Li, J. Qiao, R. Jin, Y. Yu and S. Gao, *Sol. Energy Mater. Sol. Cells*, 2015, **132**, 650-654.
20. P. Gao, H. Ma, T. Yan, D. Wu, X. Ren, J. Yang, B. Du and Q. Wei, *Dalton Trans.*, 2015, **44**, 773-781.
21. J. A. Fernandes, P. Migowski, Z. Fabrim, A. F. Feil, G. Rosa, S. Khan, G. J. Machado, P. F. Fichtner, S. R. Teixeira and M. J. Santos, *Phys. Chem. Chem. Phys.*, 2014, **16**, 9148-9153.
22. Q. Kang, Q. Cai, S. Z. Yao, C. A. Grimes and J. Ye, *J. Phys. Chem. C*, 2012, **116**, 16885-16892.
23. L. Su, J. Lv, H. Wang, L. Liu, G. Xu, D. Wang, Z. Zheng and Y. Wu, *Catal. Lett.*, 2014, **144**, 553-560.
24. J. Xue, Q. Shen, F. Yang, W. Liang and X. Liu, *J. Alloys Compd.*, 2014, **607**, 163-168.
25. J. Xue, Q. Shen, W. Liang, X. Liu and F. Yang, *Electrochim. Acta*, 2013, **97**, 10-16.
26. Y.-G. Kim, J. Y. Kim, D. Vairavapandian and J. L. Stickney, *J. Phys. Chem. B*, 2006, **110**, 17998-18006.
27. R. Vaidyanathan, J. L. Stickney and U. Happek, *Electrochim. Acta*, 2004, **49**, 1321-1326.
28. M. K. Mathe, S. M. Cox, B. H. Flowers, R. Vaidyanathan, L. Pham, N. Srisook, U. Happek and J. L. Stickney, *J. Cryst. Growth*, 2004, **271**, 55-64.
29. J. L. Stickney, *Adv. Electrochem. Sci. Eng.*, 2002, **7**, 1-106.
30. V. Venkatasamy, N. Jayaraju, S. Cox, C. Thambidurai, U. Happek and J. Stickney, *J. appl. Electrochem.*, 2006, **36**, 1223-1229.
31. J. Fang, Y. Liu and T. Chin, *Thin Solid Films*, 2015, **580**, 1-5.
32. J. Zhang, J. Yang, M. Liu, G. Li, W. Li, S. Gao and Y. Luo, *J. Electrochem. Soc.*, 2014, **161**, D55-D58.
33. R. Kowalik, in *Meeting Abstracts*, Electrochem. Soc., 2015, pp. 891-891.
34. W. Zhu, X. Liu, H. Liu, D. Tong, J. Yang and J. Peng, *J. Am. Chem. Soc.*, 2010, **132**, 12619-12626.
35. H. Wang, W. Zhu, B. Chong and K. Qin, *Int. J. Hydrogen Energ.*, 2014, **39**, 90-99.
36. B. Chong, W. Zhu, Y. Liu, L. Guan and G. Z. Chen, *J. Mater. Chem. A*, 2016, **4**, 1336-1344.
37. N. K. Allam, F. Alamgir and M. A. El-Sayed, *ACS nano*, 2010, **4**, 5819-5826.
38. C. Ma, Y. Ding, D. Moore, X. Wang and Z. L. Wang, *J. Am. Chem. Soc.*, 2004, **126**, 708-709.
39. Z. Feng, Q. Zhang, L. Lin, H. Guo, J. Zhou and Z. Lin, *Chem. Mater.*, 2010, **22**, 2705-2710.
40. P. Gao, D. Bao, Y. Wang, Y. Chen, L. Wang, S. Yang, G. Chen, G. Li, Y. Sun and W. Qin, *ACS Appl. Mater. Interfaces*, 2013, **5**, 368-373.
41. Y. Chen, S. Farrell, G. Brill, P. Wijewarnasuriya and N. Dhar, *J. Cryst. Growth*, 2008, **310**, 5303-5307.
42. L. Xu, X. Sun, H. Tu, Q. Jia, H. Gong and J. Guan, *Appl. Catal. B*, 2016, **184**, 309-319.
43. H. Chen, Z. Wei, K. Yan, Y. Bai, Z. Zhu, T. Zhang and S. Yang, *Small*, 2014, **10**, 4760-4769.
44. G. A. Snook, C. Peng, D. J. Fray and G. Z. Chen, *Electrochem. commun.*, 2007, **9**, 83-88.
45. X. Yang, L. Chi, C. Chen, X. Cui and Q. Wang, *Phys. E*, 2015, **66**, 120-124.
46. C.-W. Kung, Y.-H. Cheng, H.-W. Chen, R. Vittal and K.-C. Ho, *J. Mater. Chem. A*, 2013, **1**, 10693-10702.
47. N. Srinivasan, Y. Shiga, D. Atarashi, E. Sakai and M. Miyauchi, *App. Catal. B*, 2015, **179**, 113-121.
48. T. Abdiryim, A. Ali, R. Jamal, Y. Osman and Y. Zhang, *Nanoscale Res. Lett.*, 2014, **9**, 1-8.
49. E. Hendry, M. Koeberg, B. O'Regan and M. Bonn, *Nano lett.*, 2006, **6**, 755-759.
50. X.-F. Gao, H.-B. Li, W.-T. Sun, Q. Chen, F.-Q. Tang and L.-M. Peng, *J. Phys. Chem. C*, 2009, **113**, 7531-7535.
51. M. G. Walter, E. L. Warren, J. R. McKone, S. W. Boettcher, Q. Mi, E. A. Santori and N. S. Lewis, *Chem. Rev.*, 2010, **110**, 6446-6473.
52. G. K. Mor, K. Shankar, M. Paulose, O. K. Varghese and C. A. Grimes, *Nano Lett.*, 2006, **6**, 215-218.
53. V. Spagnol, E. Sutter, C. Debiemme-Chouvy, H. Cachet and B. Baroux, *Electrochim. Acta*, 2009, **54**, 1228-1232.
54. P. Sheng, W. Li, J. Cai, X. Wang, X. Tong, Q. Cai and C. A. Grimes, *J. Mater. Chem. A*, 2013, **1**, 7806-7815.
55. P. Wang, D. Li, J. Chen, X. Zhang, J. Xian, X. Yang, X. Zheng, X. Li and Y. Shao, *Appl. Catal. B*, 2014, **160**, 217-226.
56. F. Fabregat-Santiago, G. Garcia-Belmonte, J. Bisquert, P. Bogdanoff and A. Zaban, *J. Electrochem. Soc.*, 2003, **150**, E293-E298.